

HST/WFPC2 Images of the GG Tauri Circumbinary Disk

John E. Krist¹, Karl R. Stapelfeldt², and Alan M. Watson³

ABSTRACT

We present the first visible wavelength images of the GG Tauri circumbinary ring, obtained with the Hubble Space Telescope's Wide Field and Planetary Camera 2. Scattered light from the ring is detected in both V and I band images. The images show that the ring is smooth, except for a small gap that could be a shadow caused by material between the stars and the ring. The spokes seen extending from the stars to the ring in ground-based adaptive optics images are not seen in our data, which suggests that they may be image artifacts. The nearside/farside surface brightness ratio is 6.9 in I band, consistent with forward scattering by small dust grains. The azimuth of the peak ring surface brightness appears offset by 13° from the azimuth closest to us, as seen in previous near-IR HST observations. This may indicate that the ring is warped or somehow shadowed by the circumstellar disks. The color of the ring is redder than the combined light from the stars as observed by HST, confirming previous measurements that indicate that circumstellar disks may introduce extinction of light illuminating the ring. We detect a bright, compact arc of material $0''.3$ from the secondary star at an azimuth opposite the primary. It appears to be too large to be a circumstellar disk and is not at the expected location for dust trapped at a Lagrange point.

Subject headings: stars: circumstellar matter — stars: individual (GG Tauri) — stars: pre-main sequence — stars: binaries

¹Space Telescope Science Institute, 3700 San Martin Dr., Baltimore, MD 21218 (krist@stsci.edu)

²MS 183-900, Jet Propulsion Laboratory, Pasadena, CA 91109 (krs@exoplanet.jpl.nasa.gov)

³Instituto de Astronomía, Universidad Nacional Autónoma de México, Apartado Postal 72-3, 58089 Morelia, Michoacán, México (alan@astrosmo.unam.mx)

1. Introduction

GG Tauri (HBC 54; IRAS 04296+1725) is a young multiple star system located in the Taurus L1551 molecular cloud at a distance of 140 pc (Elias 1978). It includes two binaries, GG Tau *Aa/Ab*, with a separation of $\sim 0''.25$, and $10''.6$ away, GG Tau *Ba/Bb*, separated by $1''.5$. GG Tau *Aa/Ab* (collectively hereafter just GG Tau) is especially interesting because it possesses a circumbinary disk that has been imaged in molecular line and dust continuum emission with millimeter interferometry (Dutrey, Guilloteau, & Simon 1994, hereafter DGS94; Guilloteau, Dutrey, & Simon 1999, hereafter GDS99). Subsequently, images of the disk in scattered light were obtained in the near-infrared with ground-based adaptive optics (Roddier et al. 1996, hereafter R96) and the Hubble Space Telescope (HST) (Silber et al. 2000; McCabe & Ghez 2000).

These measurements show that the disk has a large inner hole, ~ 180 AU in radius, which has apparently been cleared by tidal interactions with the binary. While the disk has been detected out to a radius of ~ 800 AU in millimeter line emission, virtually all of the scattered light and millimeter continuum emission is confined within an annulus of radius 180-260 AU. For this reason, the disk is usually described as a ring. The morphology is consistent with a circular ring inclined $\sim 37^\circ$ from the plane of the sky. The CO kinematics are in excellent agreement with Keplerian disk models (GDS99). Redshifted gas is found along the ring’s western side, and blueshifted gas on its eastern. Assuming that the disk and binary rotate in the same direction, this information and the observed motions of the stars indicate that the northern, brighter side of the ring must be the nearest to us (R96).

The adaptive optics (AO) images of R96, which were further analyzed by Close et al. (1998), showed a clumpy ring and indicated the presence of radial “spokes” extending inward from the ring toward the central binary. Later AO images taken with Gemini (Potter et al. 2001) also contained some spokes. These features resembled predictions for accretion streams from a circumbinary disk (Artymowicz & Lubow 1994). However, both of the near-IR observations with HST (Silber et al. 2000; McCabe & Ghez 2000) show an essentially smooth ring, with no evidence for the spokes at the intensity levels indicated in the AO images.

Previous photometry of the individual binary components suggests that each may possess its own circumstellar disk. Near-infrared excesses were noted in both stars by R96. White et al. (1999) derived from HST spectra line-of-sight extinctions $A_V=0.72$ and 3.20 to GG Tau *Aa* and *Ab* respectively. This large difference between two sources just $0''.25$ (35 AU) apart (projected) shows that there must be extinction localized at one of the stars, perhaps from a small circumstellar disk. Limits to the amount of circumstellar material are provided by high resolution 2.7 mm and 1.3 mm continuum maps by Looney, Mundy, &

Welch (2000) and GDS99, respectively. These show that no more than a few percent of the total flux from the system can originate in the circumstellar material of the individual binary components. While any such disks must therefore be small and low mass in comparison to the outer circumbinary ring, their presence may have important effects on the ring’s illumination. Indeed, R96 noted that the ring was redder than the combined light from the two stars and suggested that this indicated extinction along the line of sight between the central binary and the ring. Wood, Crosas, & Ghez (1999) explored this scenario quantitatively, and through modeling of the scattered light images of R96 and ^{13}CO J=1-0 line profiles of DGS94, found that extinction from circumstellar disk(s) appeared necessary to account for the brightness and color of scattered light from the ring. Despite the many lines of indirect evidence, no resolved images of circumstellar disks in the GG Tau binary have yet been obtained.

Based on its strong IR excess and millimeter continuum flux, GG Tau was included in the Wide Field and Planetary Camera 2 (WFPC2) Investigation Definition Team’s HST observing program before the nature of the ring was confirmed by DGS94 and R96. We present these results here, the first images of the GG Tau ring at visual wavelengths.

2. Observations and Processing

GG Tau was observed using HST/WFPC2 on 27 September 1997 as part of HST program 6855. High resolution images of the binary and ring were taken at the center of the Planetary Camera (PC1, $0''.0456 \text{ pixel}^{-1}$) in F555W (WFPC2 V band) and F814W (WFPC2 I band). Short exposures (3s in F555W, 2s in F814W) provided unsaturated images of the binary for photometry, while longer exposures (two 200s in F555W and two 100s in F814W) were used for imaging the ring. In addition, short (1s), medium (40s) and long (two 300s) exposures were taken through filter F606W with GG Tau centered in Wide Field Camera 3 (WF3, $0''.1 \text{ pixel}^{-1}$), in order to maximize sensitivity to low surface brightness emission. All images were taken at a gain of 14 photons DN^{-1} , except for the longest exposure F606W images which were taken at 7 photons DN^{-1} .

The data were processed by the HST calibration pipeline, and duplicate images combined with cosmic ray rejection. In the longer exposures, the stars were saturated and there was CCD column bleeding. These saturated pixels were replaced by scaled, unsaturated values from shorter exposures. This produced images that were unsaturated beyond $0''.14$.

2.1. Point Spread Function (PSF) Photometry and Astrometry

Using a method that has been effective in the past for close binaries such as FS Tauri (Krist et al. 1998) and XZ Tauri (Krist et al. 1999), the position and intensity of each component of GG Tau was determined by simultaneously fitting simulated PSFs within 39 by 39 pixel boxes centered on the binary in the short exposures. The PSFs were generated for each filter using version 5.0c of the Tiny Tim HST PSF modeling program (Krist & Hook 2000). The models matched the reported colors (Ghez, White, & Simon 1997) of each binary component. They were subsampled by a factor of five in each dimension, allowing the fitting procedure to accurately interpolate and rebin the PSFs to match the positions of the stars in the images. Aperture corrections derived from larger PSF models were applied to the measured fluxes which were then converted to V and I_c magnitudes using SYNPHOT (Bushouse & Simon 1998), assuming an M1.5V spectral type. These values are provided in Table 1. The uncertainties include estimates of the measurement errors and errors in the conversion of fluxes to standard magnitudes. The combined magnitudes are $V=12.15$ and $I_c=10.23$ ($V-I_c=1.92$).

The measured separations are $0''.251$ (F814W) and $0''.249$ (F555W), with estimated errors of $\pm 0''.003$. The average position angle is $354.3^\circ \pm 1^\circ$. In the 3 years between our data and the September 1994 WFPC2 images of Ghez, White, & Simon (1997), the position angle has decreased by $\sim 4.5^\circ \pm 2^\circ$ ($\sim 1.5^\circ \pm 0.7^\circ \text{ year}^{-1}$) but the separation has not measurably changed. This agrees with the astrometric results compiled by Woitas, Köhler, & Leinert (2001). The combined mass of GG Tau *Aa* and *Ab* is $1.28 \pm 0.07 M_\odot$, as inferred from the ring kinematics by Simon, Dutrey, & Guilloteau (2000). The mean angular velocity for a circular binary orbit with this mass and semi-major axis of 18 AU (22 AU deprojected; $d=140$ pc) is 4.0° (2.8°) per year. The observed rate is much less than this, so the orbit is likely to be eccentric ($e > 0.25$) and observed near apoastron (assuming that the binary and ring are coplanar).

In addition to the PSF-fitting photometry of *Aa/Ab*, we also used aperture photometry to measure the fluxes of the GG Tau *Ba/Bb* stars, which are shown in Table 1. Conversions to standard magnitudes were done using SYNPHOT and an M5.5V spectrum. GG Tauri *Bb* is especially red compared to the other stars and has been identified as a possible young brown dwarf (White et al. 1999).

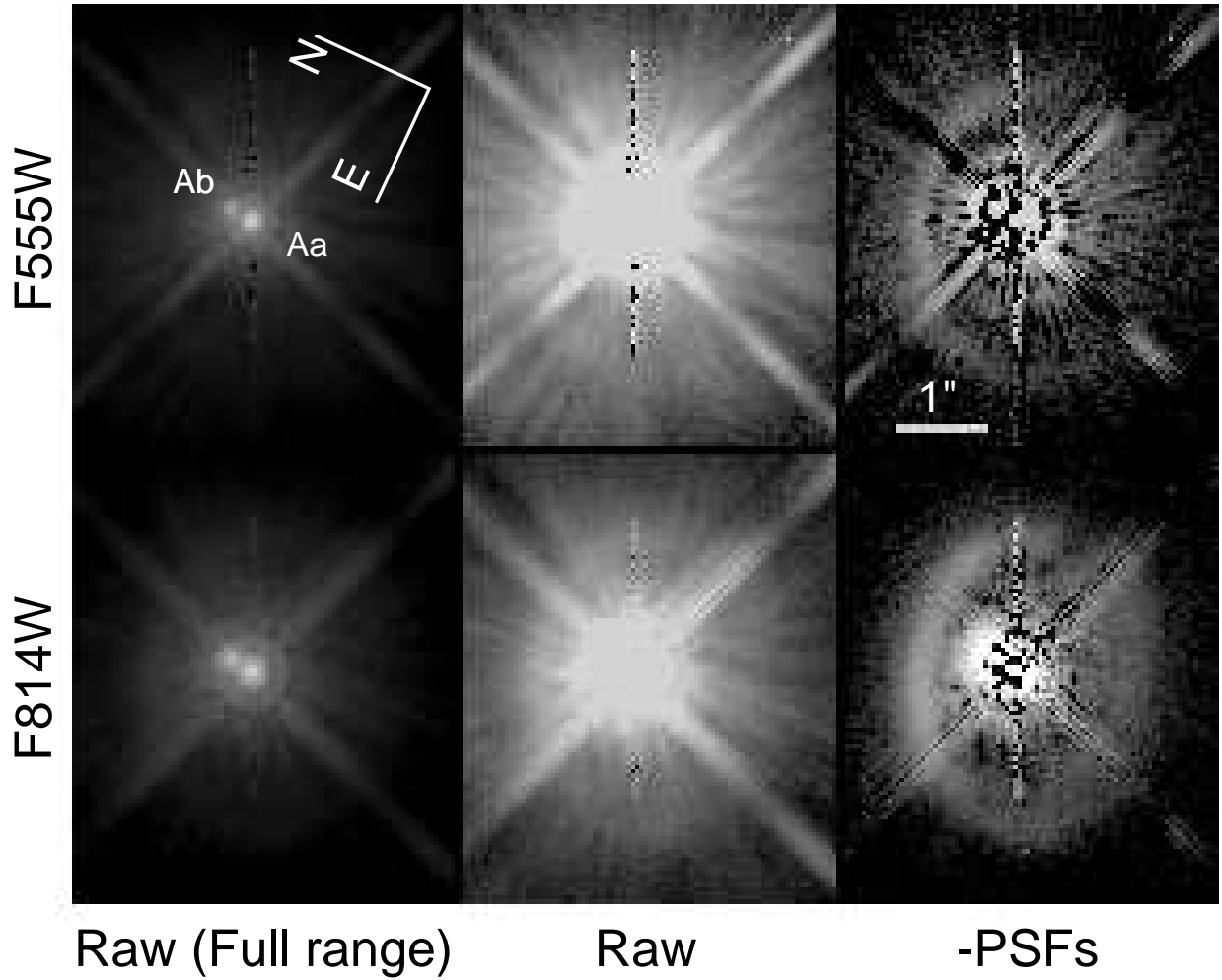


Fig. 1.— HST/WFPC2 Planetary Camera ($0''.0456 \text{ pixel}^{-1}$) images of GG Tauri before and after PSF subtraction (logarithmic stretches). On the left are the images displayed over their full range. The middle and right frames are identically stretched to emphasized low-brightness features.

2.2. PSF Subtraction

The ring intensity in the long exposures was just above or equal to the local background level, which was dominated by the wings of the combined point spread functions (Figure 1). PSF subtraction was required to provide a clear view of the ring. This is complicated by the optical characteristics of HST and WFPC2, which cause the PSF to be dependent on position, focus, and color, introducing potential mismatches between target and reference images. The best subtractions are obtained using images of isolated stars that have similar colors and exposure levels, and which are imaged near (within $1''$) the same detector location as the target. At radii beyond $\sim 0''.3$, the model PSFs produced by Tiny Tim do not match as well as observed PSFs. Therefore, we selected a few isolated star images from other HST programs that matched the GG Tau observations in color, exposure level, and position on the detector.

All of the reference PSFs were saturated, with no short exposures to provide direct measurements of their intensities. We thus resorted to combining aperture photometry (excluding the saturated pixels) with assumed electron well-depths for saturated pixels to derive fluxes (Gilliland 1994). These values were then used to normalize the reference PSFs to match the fluxes of the GG Tau components in the long exposures. A binary PSF reference image was created by taking the reference PSF and coadding it with a version of itself that was offset and scaled to match the two components of GG Tau. This was then aligned with the observed image by eye using cubic convolution interpolation. The registrations appeared to be accurate to within 0.05 pixels.

In F814W, there was large selection of archived PSFs from which to choose. Two stars provided good matches to GG Tau in terms of field position and color : DQ Tauri and HD 181204. Both have M0V spectral types and are located within $0''.8$ of GG Tau’s detector coordinates. DQ Tau is a spectroscopic binary with a sub-milliarcsecond separation, so it appears as an unresolved system on PC1. The image of HD 181204 was more deeply exposed than DQ Tau’s, with saturated pixels extending $0''.25$ from the core. Saturated pixels in this frame were replaced by those from an image of DQ Tau that was appropriately shifted and intensity-scaled. This produced a combined reference PSF that had high signal in the wings but had only a small number of saturated pixels in the core, making it suitable for use to within about $0''.1$ of the GG Tau stars.

The only good match to GG Tau in F555W was an image of LkCa 15, a K5V star whose position on the detector was 34.4 pixels ($1''.6$) from GG Tau’s. LkCa 15 has a circumstellar disk which is seen from low latitudes, and which was recently detected in scattered light using deep, dual-channel polarization, adaptive optics images using the Gemini telescope (Potter et al. 2001). We failed to detect the LkCa 15 disk in this and other filters (F814W

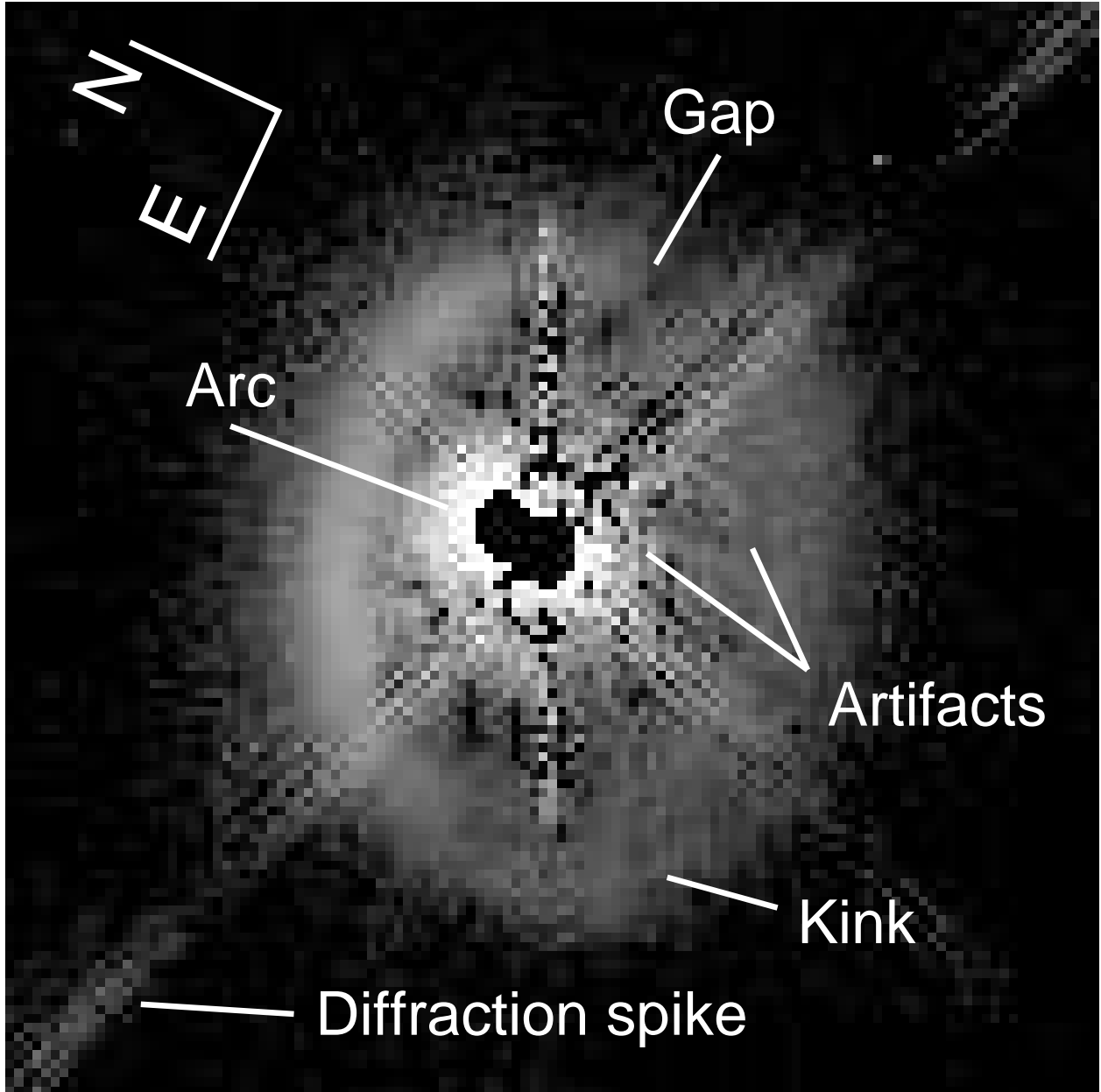


Fig. 2.— PSF-subtracted F814W image of the GG Tau ring, with various features identified. The orientation is the same as in Figure 1. Saturated pixels in the core of GG Tau have been masked.

and F675W), likely due to the short exposures used. Given that the LkCa 15 scattered light disk is small (diameter of $\sim 1''$, less than the central hole in the GG Tau ring) and within the level of the noise, it seemed relatively safe to use it for subtraction, and it was the only reasonable match.

The F814W subtractions produced good images of the ring, which is reliably seen at all azimuths, excluding the diffraction spike locations. The ring interior is also largely free of artifacts. There is a small PSF residual ring around the brighter star (identified as an artifact in Figure 2). The circumbinary disk in F814W is much better exposed than in F555W, due to the greater brightnesses of the stars in the longer wavelength passband. The estimated detection limit (3σ above the background) at $1''$ is $I_c = 18.5 \pm 0.25 \text{ mag arcsec}^{-2}$, based on an analysis of a large number of PSF subtractions that will be presented in a future paper (Stapelfeldt, private communication).

The F555W subtraction is strongly contaminated by residuals due to mismatches in both the colors and field positions of the target and reference PSFs. The northern edge of the ring is sufficiently bright to dominate over the residuals, except in the regions of diffraction spikes. The southern edge, however, is clearly dominated by residual streaks and ringing patterns characteristic of PSF mismatches, and so any detection of the ring in that region is suspect. The interior of the ring in this filter is likewise filled with residuals, none of which should be mistaken for physical structures. We were unable to derive a good estimate of the detection limit for this image due to the large PSF-related residuals but assume that it must be brighter than $V=20 \text{ mag arcsec}^{-2}$, based on the residual brightness in the far side of the ring. We strongly urge observers with future high-contrast programs on WFPC2 to avoid our problems and obtain a reference PSF of the appropriate color at a number of positions around ($\sim 0''.5$ away from) the planned target position, which will allow them to select the best match in terms of location.

Unfortunately, we could not find in the HST archive an observed PSF for the WF3 F606W subtraction that suitably matched the color, field position, and exposure level of GG Tau. Therefore, only the F555W and F814W Planetary Camera images are discussed further.

3. Results

The raw and PSF-subtracted data are shown in Figure 1. The PSF-subtracted images reveal a generally smooth ring, with no prominent clumps. A major feature of the ring is the broad azimuthal brightness peak along its northern edge. As noted by Silber et al. 2000,

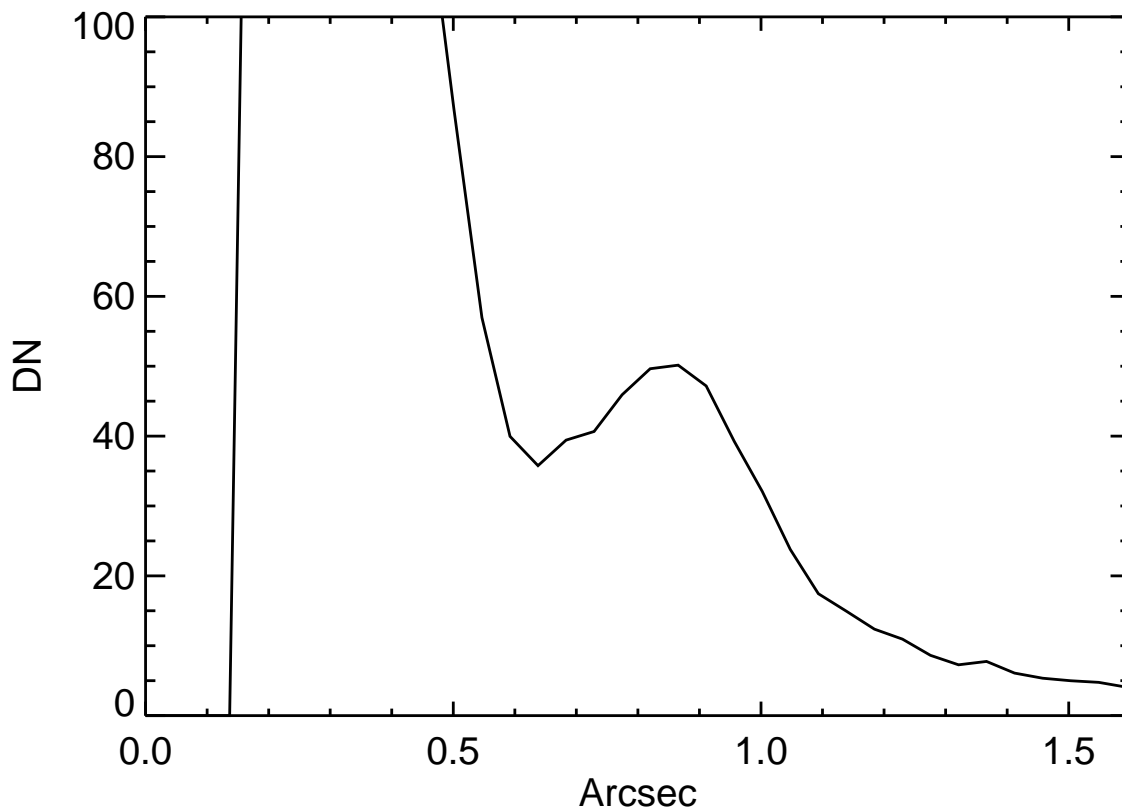


Fig. 3.— Radial intensity cut through the PSF subtracted F814W image of the circumbinary ring. The cut is taken along an axis passing through the brightest part of the ring and spans position angles 14-22°. The linear distance and PAs are expressed relative to the midpoint between the two stars, and the amplitude is given in detector counts (proportional to photons). The ring corresponds to the peak at $r=0.85$ arcsec; the relatively broad profile is apparent. Emission at $r < 0.5$ arcsec traces the arc near the secondary, and PSF residuals. Saturated pixels at $r < 0.15$ arcsec have been blanked out.

this is almost certainly due to the forward scattering properties of small dust particles within the ring. Its radial intensity cross-section there is approximately Gaussian, with a FWHM of $0''.3$ (Figure 3). The surface brightness decreases by nearly a factor of two between the brightest portion of the northern section of the ring inwards to the darkest region of the clearing, a span of $0''.15$ (20 AU). The contrast is probably larger than this, as PSF residuals may dominate the surface brightness within the clearing.

The southern section of the ring appears about twice as broad as the northern. This is expected as we are seeing both the illuminated inner wall and upper surface of the ring towards the south, as discussed by R96 and Silber et al. (2000). The eastern extreme of the ring appears to have a broader radial distribution than the western side, which is more narrowly peaked. There is a slightly dark, azimuthal band in the southern side in F814W at $r=1''.1$ that corresponds to a diffraction feature seen in the reference PSFs and is not real (i.e. it is likely not a shadow cast by a disk around one of the stars). It is identified as an artifact in Figure 2.

There is a $\sim 0''.4$ wide gap in the eastern section of the ring centered at $PA \approx 268^\circ$ (Figure 2). Its apparent southern edge is adjacent to a PSF diffraction spike artifact, so its full width cannot be determined from our images. It is seen both in F555W and F814W and is also apparent in the HST images of Silber et al. (2000) and adaptive optics images (Potter et al. 2001; Tamura et al. 2001). The brightness decreases by at least a factor of four within the gap relative to the expected trend across this section of the ring. At first glance it appears to be aligned towards the secondary star, GG Tau *Ab*, but this could simply be a projection effect as we are seeing both the inner wall and upper surface of the ring at that position.

Plots of the azimuthal ring surface brightness profiles are given in Figure 4. They were derived by computing the mean intensity in 3 by 3 pixel boxes along an ellipse that was manually constrained to pass through the region of peak radial brightness at each azimuth around the ring. These values were converted to V and I_c surface brightnesses in the same way as the stellar fluxes. The profile shapes generally match between the two filters, though the surface brightness in F555W is lower. It is unclear if the F555W brightness in the southern part of the ring is a secure detection - it is probably artificially high there due to the PSF subtraction residuals. Except for this region, the ring has an overall V-I color of 2.7 mag, 0.8 mag redder than the combined stellar flux. The gap is evident in these plots between $PA=265-280^\circ$, as marked in Figure 4.

The general peak intensity occurs at $PA \approx 25^\circ$, in agreement with Silber et al. (2000). This does not coincide with the nearest edge of the ring, which is at $PA=7^\circ$ as determined from mm observations (GDS99). The minimum lies between PAs of $130-170^\circ$, in a portion of the ring where the azimuthal intensity trend is disrupted (a region that Silber et al. identified

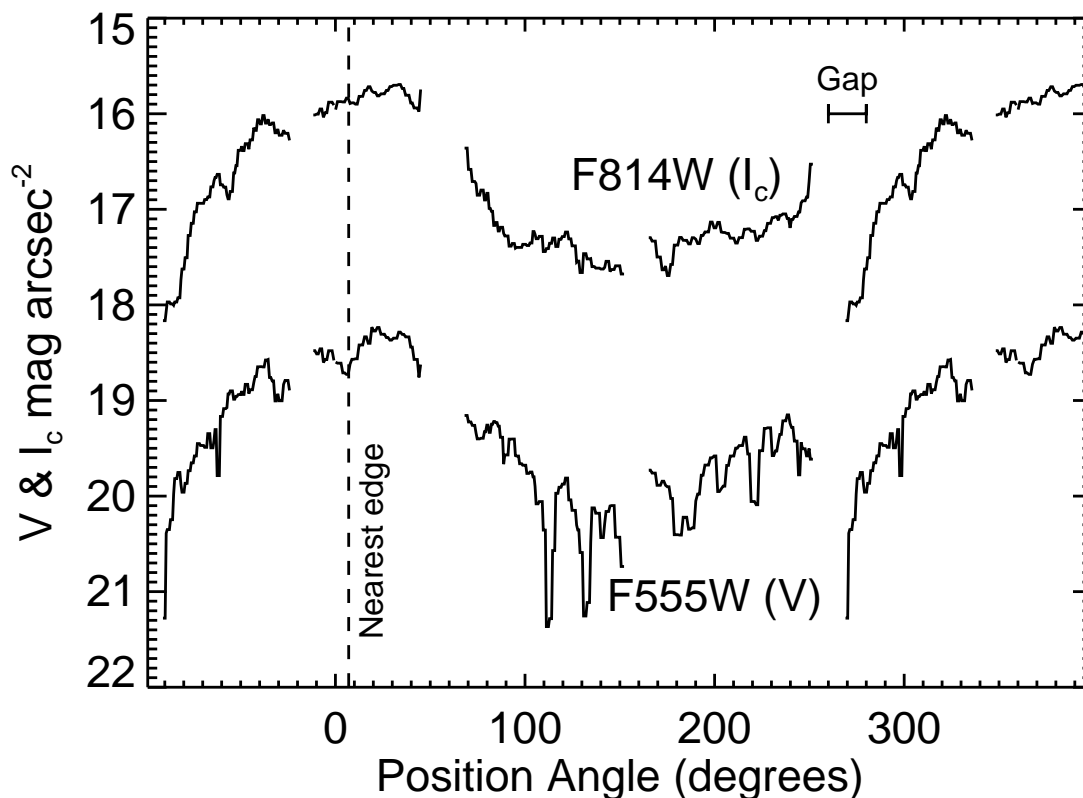


Fig. 4.— Azimuthal profile plot of the GG Tau ring. The values plotted are the mean surface brightness in a 3 by 3 pixel ($0''.14$ by $0''.14$) aperture along an ellipse visually constrained to fit the ring. Regions of no data are the locations of the diffraction spikes. The F555W plot has a number of sharp local minima which are subtraction artifacts. The position angle is measured relative to the midpoint between the two stars. Note that the surface brightness of a PSF with the combined flux of both stars light at $1''$ is $V=17.5$ and $I=15.3$ mag arcsec⁻². The profiles have been replicated to extend the plots beyond 0° - 360° . The position angle of the nearest edge of the ring as determined from radio emission measurements is marked with a dashed line. The mean color difference is $V-I_c=2.7$.

as a “kink”; see Figure 2). The maximum and minimum surface brightnesses around the ring have a ratio of 6.9 in F814W, greater than the value of ~ 4.0 at $1.2 \mu\text{m}$ measured by Silber et al., or the 5.0 at $1.6 \mu\text{m}$ from McCabe & Ghez 2000). This ratio is expected to increase with decreasing wavelength as forward scattering becomes stronger, assuming that the bulk of the dust consists of $< 0.6 \mu\text{m}$ particles.

The interior of the ring, at least in the relatively clean F814W subtraction, is brighter than the background outside of the ring, and it appears clear of any physical structures except for a small arc (discussed below). The interior surface brightness is $I_c < 18 \text{ mag arcsec}^{-2}$ (the large residuals in F555W are too great to deduce an accurate interior brightness). It is not clear whether this flux is due to subtraction residuals or scattering material. This amount of flux cannot, however, be explained by the convolution of the instrumental PSF with the ring. We do not detect the bright artifact Silber et al. saw in their subtraction at $\text{PA}=144^\circ$ midway between the stars and the ring. Unless it was a transient feature, we should have seen it, as it was brighter than the nearby section of the ring. Two circular rings appear around the stars in both filters, and are definitely subtraction artifacts. There are no indications of bright spokes interior to the ring like those seen in the AO images of R96 (though one of their spokes would lie under the region in our images contaminated by saturated column residuals).

In the F814W image there is a bright, compact structure adjacent to GG Tau *Ab* that extends $\sim 0''.3$ towards the north from the star. It has an arc shape (see Fig. 2), and is roughly symmetric about $\text{PA} \approx 0^\circ$. Its surface brightness decreases from $I_c = 12.7$ to 16.5 mag arcsec ($\pm 0.8 \text{ mag}$) between $0''.2$ – $0''.6$. Within $0''.2$, the stellar subtraction residuals are too great to obtain a good measurement, and residuals may dominate out to approximately $0''.4$. The circumbinary ring dominates past $0''.6$. A similar arc can be seen in the Silber et al. (2000) NICMOS images, though they do not point it out and presumably believed it to be a subtraction artifact. It is not seen in the NICMOS images of McCabe & Ghez (2000), which have significant subtraction residuals near the stars and lower resolution. Likewise, we are unable to positively identify it relative to the large residuals in our F555W image. To investigate the potential that this arc could be a subtraction residual like the ring seen around the primary in Figure 2, we generated a number of Tiny Tim model F814W PSFs for a reasonable selection of object colors (K5V–M3V, including extinction), telescope focus offsets (0 – $6 \mu\text{m}$ breathing), and normalization errors (1–20%), and then subtracted each from the others. We were unable to duplicate this feature in form or relative brightness. Likewise, the Silber et al. NICMOS images should not be biased by similar effects. These experiments, and the fact that the same structure is seen in the NICMOS data, lead us to conclude that it is actually reflecting material near GG Tau *Ab*.

4. Discussion

4.1. Constraints on the current ring model

The prevailing model for the GG Tau circumbinary disk is a vertically thick, inclined circular ring with a completely cleared central hole and illuminated by reddened starlight. The WFPC2 images, as the highest spatial resolution images yet obtained of the ring, and as the first taken at wavelengths below $1\ \mu\text{m}$, provide new tests for this general picture. We now discuss the implications of the WFPC2 data for the prevailing ring model.

4.2. Ring geometry

The isophotes in the F814W image were visually fitted with ellipses to characterize the *apparent* ring geometry. One focus of an ellipse was fixed at a location 46% of the way from the primary to the secondary star, in accordance with the inferred stellar mass ratio (White et al. 1999). The best-fit parameters were: inner edge semi-major axis of $1''.27$ (180 AU); outer edge semi-major axis of $1''.73$ (240 AU); and a ring inclination 37° from face-on. The center of the projected ellipses is offset $0''.26$ S of the binary center of mass. In the case of a completely flat, elliptical ring this would be a physical offset, and an intrinsic ring eccentricity of 0.21 would be required. However, it is much more likely that the ring has a significant vertical thickness that is 10-20% of its radius. In this case, even an intrinsically circular ring can exhibit an offset in the center of its scattered light from its central star(s). In GG Tau the apparent offset is in the direction expected for the latter case (GDS99). Therefore, the offset of the ring center from the binary is not a compelling reason to ascribe any intrinsic eccentricity to the circumbinary ring. Uncertainty in the precise value of the ring thickness prevents us from drawing any conclusions about the ring eccentricity from simple ellipse fitting.

The azimuthal distribution of light in the ring is somewhat of a mystery. CO kinematics indicate that the near side is located at $\text{PA}=7^\circ$. In a symmetric, circular ring with forward-scattering dust grains, the brightest azimuth would be expected to align exactly at this position angle, but in GG Tau it does not. Instead, the azimuth of peak brightness is offset $\sim 13^\circ$ E from this, as determined by visually fitting a curve to the brightest section of the azimuthal profile. A curve fit to a larger section ($\text{PA}=-80^\circ$ to 90°) peaks at about 7° , as expected, indicating that the offset is a localized phenomenon. The effect of binary illumination should not shift the azimuth of peak brightness significantly from the expected value, as discussed below. Shadowing by a non-coplanar disk or perhaps the material seen near the secondary might result in the offset. Another explanation might be an intrinsic

ring eccentricity. In this case, the azimuth of peak brightness would be offset away from the PA of the near edge and toward the PA of ring periaapse. While this possibility cannot be discounted, other evidence for ring eccentricity would be needed to establish it.

Comparison of scattered light models with optical HST disk images has proven to be a valuable way to constrain the disk density distributions and dust properties (Burrows et al. 1996; Stapelfeldt et al. 1998). Unfortunately it was not practical for us to determine an optimal model for the GG Tauri ring. The key problem is uncertainty in the relative contributions of each star to the ring illumination. At one extreme is the possibility that one star dominates the ring illumination, as suggested by the fact that the primary appears > 1.5 mag brighter than the secondary at optical wavelengths. At the other extreme is the possibility that each star makes a roughly equal contribution to the ring illumination, as suggested by the fact that the components have comparable intrinsic brightnesses after correction is made for extinction (White et al. 1999). Given this range of uncertainty, we did not attempt to identify a fully optimized scattered light model for GG Tauri. Instead, we chose only to validate the disk density distribution determined by GDS99 as a consistency check with the WFPC2 images. To do this, we used the PINBALL Monte Carlo multiple scattering code (Watson & Henney 2001) to calculate model ring images at $\lambda = 0.8 \mu\text{m}$. An inclined circular ring was illuminated by identical binary point sources whose deprojected positions were consistent with the parameters of GG Tau.

In these simulations, the GDS99 density law provides a good match to the morphology of the WFPC2 image. This model is shown in Figure 5. Through trial and error, we found that a Henyey-Greenstein phase function asymmetry parameter $g=0.65$ provided the best match to the observed brightness ratio between the front/back sides of the ring. This value is in excellent agreement with determinations made in the disks of HH 30 (Burrows et al. 1996) and HK Tau/c (Stapelfeldt et al. 1998). Finally, our simulation shows that even a continuous disk extending from $180 \text{ AU} < r < 800 \text{ AU}$ is dominated by a bright inner ring of light like that seen in GG Tau. Both the WFPC2 data and the scattered light model show that on disk’s N side, the surface brightness drops by an order of magnitude just $0''.3$ outside the radial peak emission of the bright ring. No density discontinuity or enhanced shadowing is needed to account for the different outer radii measured in scattered light and millimeterwave CO emission; such a sharp drop in surface brightness with radius is expected, even for a continuous disk.

For the assumed case of equal binary illumination, the distribution of light on the ring appears nearly the same as for the case where the ring is illuminated by a single central point source. This result can be readily understood analytically. The peak-to-valley deviation of the disk azimuthal brightness profile in a coplanar binary model with both stars of equal

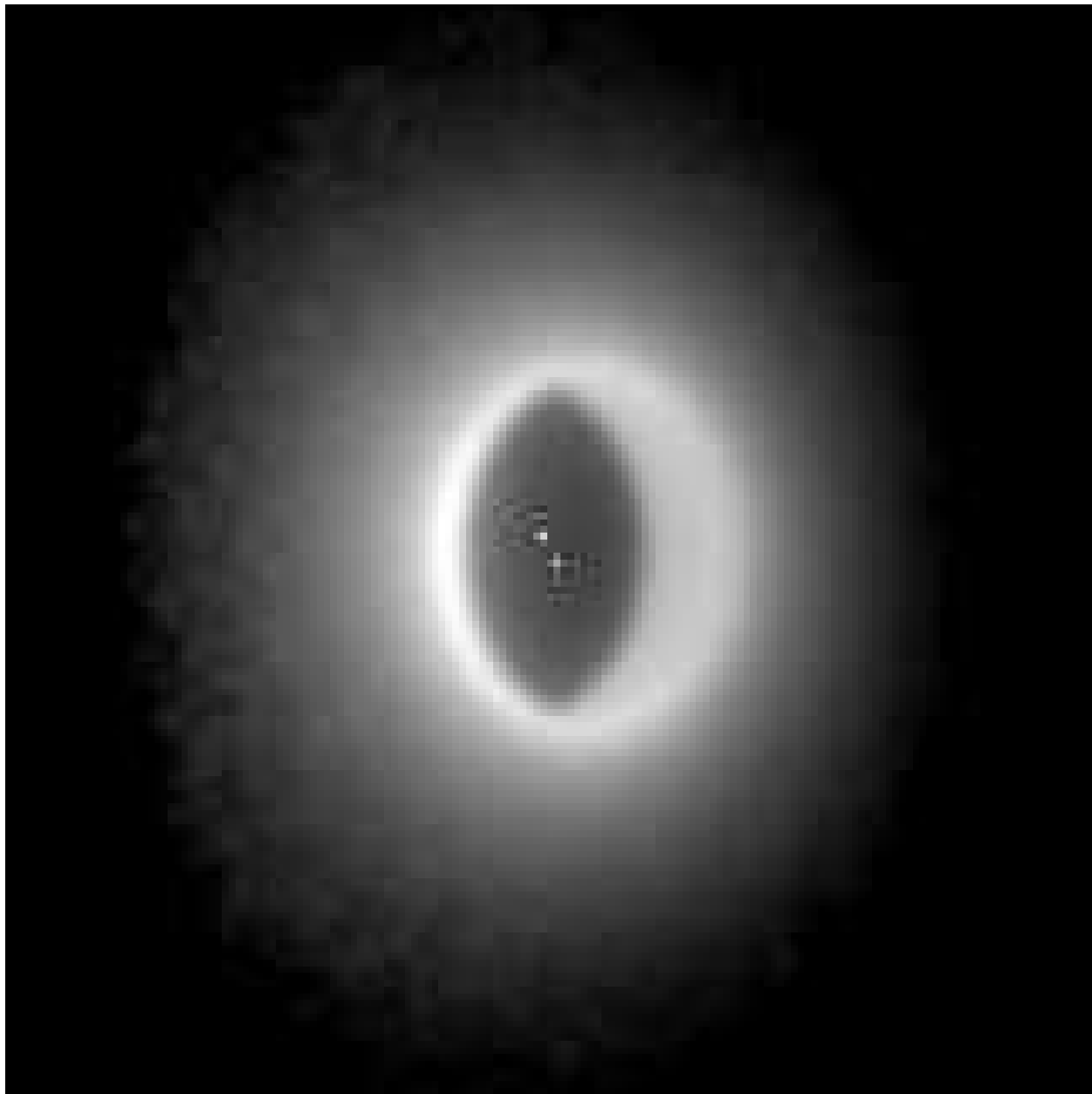


Fig. 5.— Monte Carlo multiple scattering model of the GG Tauri circumbinary disk, displayed with a logarithmic stretch and with a similar orientation as the ring shown in Figures 1 and 2. Illumination from equally bright binary components was assumed (no circumstellar disks). The model parameters are: inner radius = 180 AU; outer radius = 800 AU; scale height = 40 AU at 300 AU; disk mass = $0.12 M_{\odot}$; scale height scales with radius as $r^{1.05}$; midplane volume density scales with radius as $r^{-2.75}$; dust opacity $120 \text{ cm}^2 \text{ gm}^{-1}$; scattering phase function asymmetry parameter $g = 0.65$; inclination is 37° ; and 190 million photons traced. Dots mark the positions of the stars. The disk model (but not the stars) was convolved with a Tiny Tim model PSF for filter F814W.

brightness compared to a single-star model is $\mathcal{R} = [(R + d)^2 + (R - d)^2]/2R^2$, where R is the disk inner radius and d is half the binary separation. Defining $x \equiv d/R$, then $\mathcal{R} = [(1 + x)^2 + (1 - x)^2]/2 = 1 + x^2$. For the case of GG Tau, $R = 180$ AU at the ring inner edge, and $d = 22$ AU (deprojected): thus, the peak-to-valley variation is only 3% around the ring. The peak-to-valley deviation of disk brightness in a coplanar binary model with one dominant star compared to a single-star model is $\mathcal{R} = (R + d)^2/R^2$, which reduces to $1 + 2x$. This would produce a 40% peak-to-valley effect. Thus, the surface brightness of the disk will only differ significantly if one star (as seen by the disk) is much brighter than the other.

4.3. Ring photometry

The reflected light from the ring appears redder than the direct starlight in the WFPC2 optical images, continuing the trend first identified in the near-infrared by R96. In an optically thick disk like that of GG Tau, the color of reflected starlight should be very similar to the color of the source(s) which illuminate it. The color difference between the disk light and the direct starlight ($V-I = 0.8$ mag) therefore requires that light seen by the disk be reddened by an additional $A_V \geq 1.2$ mag with respect to the direct light seen by an earthbound observer (assuming a standard extinction law). Wood, Crosas, & Ghez (1999) have shown that such an extinction can be readily produced by circumstellar disks surrounding one or both of the central binary components.

We searched for color gradients in the ring using a smoothed F555W/F814W ratio image. Two possible mechanisms might produce observable color gradients in the ring: (1) Any regions with enhanced shadowing would be expected to appear redder than the rest of the ring; and (2) the expected wavelength dependence in the dust phase function should cause the near (N) side of the ring to appear more blue, and the far (S) side to appear redder, than the ring as a whole. Unfortunately we were not able to identify any color gradients in the ring because of the low signal-to-noise and large PSF subtraction residuals in our F555W image.

4.4. Ring substructure

The WFPC2 and NICMOS images indicate that the GG Tau ring is essentially smooth and not clumpy as the adaptive optics (AO) images of R96 would indicate. Also, the spokes seen in the AO images, some of which are significantly brighter than the ring, are not apparent. These clumps and spokes may be instrumental artifacts. AO systems can produce

artificial structures around bright stars, especially when deconvolution techniques are employed. The brightest spoke in the AO images, which connects the stars to the northern, bright edge of the ring, may actually be a merge of the flux from the ring and the material that we see adjacent to GG Tau *Ab*.

The gap in the ring surface brightness at PA=268° is reminiscent of the azimuthal density structure predicted for the case of a low mass companion embedded within a circumstellar debris disk (Liou & Zook 1999). Without dynamical forcing, any sharp azimuthal density structure corresponding to the gap would be disrupted by Keplerian shear in a few orbital timescales. Also, there are no indications of a gap in the millimeter data. An alternative possibility is that the gap represents some kind of shadow cast onto the ring by intervening, material, unseen in our images, lying between it and the illuminating stars. The shadow would have to block the illumination of the brightest component of the binary, otherwise it would not be possible to produce the observed brightness deficit of >1 mag in the gap. Furthermore, it would be necessary to assume that one star dominates the illumination of the outer ring - otherwise the gap would be filled in by the illumination of the other binary component. With these caveats, there are three possibilities for the nature of the shadowing material, none of which is fully satisfactory. The first possibility is that of a small circumstellar disk at the brightest binary component, extending along PA=268°, and inclined by a large angle to the plane of the outer ring. Illumination of the outer ring along the midplane of this circumstellar disk would be suppressed, leading to a darkened gap along the line of intersection between the outer ring and inner disk planes. While this model would do a nice job explaining the observed gap, it also predicts that a second, diametrically opposed gap should be present. This is not observed. A second, more ad-hoc possibility is to postulate a circumstellar disk coplanar with the outer ring, and with a large azimuthal density enhancement that shadows the outer ring to produce the gap. Finally, if mass transfer from the outer ring to the inner circumstellar disks were actually taking place, it is possible to imagine a dense clump in the accretion stream that might shadow the outer ring. With none of these explanations finding immediate support in the available data, for now the gap's origin must remain a mystery.

4.5. Circumsecondary material

The WFPC2 F814W observations show an arc of nebulosity located near the secondary star and well within the circumbinary ring. Given the strong artifacts present in the image just 0".3 from the secondary, it is unclear whether this nebulosity is part of a continuous distribution of material extending outward from the secondary, or a localized clump. If

continuous, then a natural explanation would be a circumstellar disk surrounding GG Tau *Ab*. The infrared excess and strongly localized extinction indicate a significant amount of dust near this star. A circumstellar disk coplanar with the ring would appear brightest on its N side because of enhanced forward scattering, exactly where the arc feature is found. However, the feature’s location ($0''.3$ outward from the secondary) implies an extent considerably larger than expected for a disk, whose maximum outer radius should be 3-5 times smaller than binary separation (i.e., ≤ 0.1 arcsec) due to tidal truncation. While this feature is small, it is still much larger than the core of the WFPC2 PSF - so even such a barely resolved disk could not plausibly extend to this radius when convolved with the PSF.

The location of this reflecting material suggests another possible explanation, that of material moving in a two body potential. The binary’s Lagrange stability point L2 is located on the line passing through the two stars, and on the opposite side of the secondary from the primary - near the location of this nebular arc. In a binary with the relative stellar masses inferred for GG Tau, this stability point would be located opposite the primary and offset from the secondary by 67% of the primary-secondary separation (Taff 1985). Since the material near the secondary is displaced from the star by more than this expected value ($0''.3$ versus $\sim 0''.17$), it appears that this is also not a satisfactory explanation for the nature of the nebular arc.

4.6. Monitoring possible time variations

Multiple-epoch observations of circumstellar disks (Watson et al. 2000; Wood et al. 2000) indicate that shadowing from variations in the dust density distribution in the inner disk, or beaming from accretion hot spots at the stellar surface, can significantly alter the light distribution in the outer disk, with timescales of hours to years. In the case of GG Tau, where shadowing by circumstellar disks may be necessary to explain the properties of the circumbinary ring, there may likewise be time-variable illumination effects. Orbital timescales in the circumstellar disks are on the order of 30 years, so the motion of any shadow patterns might be discernible in just a fraction of this period. In addition, a section of the ring may also reflect variations in the brightness of the star closest to it, skewing the front/backside brightness ratio or the azimuthal ring profile. Possible orbital motion of the dust in the arc near the secondary would also be worth investigating, as it would have a timescale on the order of a few decades. It would be interesting to monitor any such changes in the GG Tau system on long and short timescales using HST, adaptive optics, or in the future with the Next Generation Space Telescope.

5. Conclusions

HST/WFPC2 V and I band images of GG Tau resolve the binary star and reveal the scattered light from the circumbinary dust ring that was previously detected in the near-IR. The images confirm that the northern, nearer side of the ring is brightest, as is expected from forward scattering by dust grains. The nearside/farside brightness ratio is 6.9 in the I band. This effect has been reproduced using three-dimensional scattering models of the ring. The $V-I_c$ color of the ring relative to the binary colors indicates that some amount of extinction must be introduced by material between the stars, as first pointed out by R96. The new images show a clump of reflecting material near the secondary star, also seen in the Silber et al. (2000) HST images (though apparently not noticed by them), that could possibly create shadows on, or at least introduce partial extinction to, the ring. Clear evidence for shadowing is provided by a narrow gap in the ring, which has also been seen in HST/NICMOS and adaptive optics images. However, we cannot determine what may be causing this shadow, nor why it is only seen on one side if it is created by a circumstellar disk. Other brightness asymmetries, such as the differences in the eastern and western ring radial profiles, and the offset of the ring peak brightness from the closest edge, might be explained by shadowing or possibly by warping of the ring. The observations highlight the fact that the poorly understood interaction of light from the binary with ring material and possible circumstellar disks is the primary limitation to modelling the dust distribution as derived from scattered light images.

We find no evidence in our images for the “spokes” or ring clumpiness seen in the adaptive optics observations of R96. We believe that these may be AO artifacts. However, we do see some indication that the interior of the ring may not be completely clear, as there is a generally uniform distribution of light within the ring that is above the background level. More observations are required to verify whether this is reflective material or simply a PSF subtraction residual.

Higher resolution imagery, which may provide details of the circumstellar disks, should substantially improve our understanding of GG Tau. Ground-based adaptive optics imaging will help, but as demonstrated by the possible artifacts in the R96 images, any details will need to be confirmed by other systems. In the near future, the Advanced Camera for Surveys (ACS) on HST will provide high resolution ($0''.025$ arcsec pixel $^{-1}$) visible- wavelength frames with a non-field-dependent PSF, which should improve PSF subtraction results compared to WFPC2. GG Tau has been included in the ACS Science Team’s program. Further into the future, observations with ALMA (Atacama Large Millimeter Array) should provide high resolution ($0''.01$ - $0''.1$) maps of disk emission, avoiding the complications introduced by shadowing and extinction in scattered light images.

6. Acknowledgements

The GG Tauri data were taken as part of the WFPC2 Science Team’s program. Observations were made with the NASA/ESA Hubble Space Telescope, obtained from the Data Archive at the Space Telescope Science Institute, which is operated by the Association of Universities for Research in Astronomy, Inc., under NASA contract NAS 5-26555.

Table 1. Photometry of GG Tauri Stars and Disk Features.

Object	V (mag)	I _c (mag)	V-I _c (mag)
GG Tau Aa	12.25±0.03	10.47±0.03	1.78
GG Tau Ab	14.70±0.06	11.98±0.04	2.72
GG Tau Ba	17.11±0.07	13.56±0.06	3.55
GG Tau Bb	19.94±0.08	15.55±0.07	4.39
Ring (PA=20°) ¹	18.40±0.08	15.57±0.09	2.83
Ring (PA=142°) ¹	>20.29±0.50	17.75±0.20	>2.54
Ring (PA=187°) ¹	>20.10±0.50	17.35±0.20	>2.75

¹Values are mag arcsec⁻².

REFERENCES

- Artymowicz, P., & Lubow, S. H. 1994, *ApJ*, 421, 651
- Burrows, C.J., & the WFPC2 IDT 1996, *ApJ*, 473, 437
- Bushouse, H., & Simon, B. 1998, *Synphot User's Guide*, Space Telescope Science Institute
- Close, L.M., Dutrey, A., Roddier, F., Guilloteau, S., Roddier, C., Northcott, M., Ménard, F., Duvert, G., Graves, J.E., Potter, D. 1998, *ApJ*, 499, 883
- Dutrey, A., Guilloteau, S., & Simon, M. 1994, *A&A*, 286, 149
- Elias, J. H. 1978, *ApJ*, 224, 857
- Ghez, A.M., Weinberger, A.J., Neugebauer, G., Matthews, K., & McCarthy, D.W., Jr. 1995, *AJ*, 110, 753
- Ghez, A.M., White, R.J., & Simon, M. 1997, *ApJ*, 490, 353
- Gilliland, R.L. 1994, *ApJ*, 435, L63
- Guilloteau, S., Dutrey, A., & Simon, M. 1998, *A&A*, 339, 467
- Krist, J.E., Stapelfeldt, K.R., Burrows, C.J., & the WFPC2 Science Team 1998, *ApJ*, 501, 841
- Krist, J.E., Stapelfeldt, K.R., Burrows, C.J., Hester, J.J., Watson, A.M., & the WFPC2 Science Team 1999, *ApJ*, 515, L35
- Krist, J., & Hook, R. 2000, "Tiny Tim User's Guide v5.0c"
- Liou, J.-C., & Zook, H.A. 1999, *AJ*, 118, 580
- Looney, L.W., Mundy, L.G., & Welch, W.J. 2000, *ApJ*, 529, L477
- McCabe, C., & Ghez, A.M. 2000, in *IAU Symposium 200, Birth and Evolution of Binary Stars*, ed. B. Reipurth & H. Zinnecker (Potsdam), 80
- Potter, D., Baudoz, P., Guyon, O., Brandner, W., Close, L., Graves, J.E., & Northcott, M. 2001, *BAAS*, 198, 18.02
- Roddier, C., Roddier, F., Northcott, M.J., Graves, J.E., & Jim, K. 1996, *ApJ*, 463, 326
- Silber, J., Gledhill, T., Duchêne, G., & Ménard, F. 2000, *ApJ*, 536, L89

- Simon, M., Dutrey, A., & Guilloteau, S. 2000, *ApJ*, 545, 1034
- Stapelfeldt, K.R., Krist, J.E., Ménard, F., Bouvier, J., Padgett, D.L., & Burrows, C.J. 1998, *ApJ*, 502, L65
- Taff, L.G. 1985, *Celestial Mechanics* (New York:Wiley & Sons)
- Tamura, M., Suto, H., Murakawa, K., Hayashi, S., Kaifu, N., Itoh, Y., Fukagawa, M., Oasa, Y., & Naoi, T. 2001, *BAAS*, 198, 77.04
- Watson, A.M., Stapelfeldt, K.R., Krist, J.E., & Burrows, C.J. 2000, *BAAS*, 197, 47.03
- Watson, A.M., & Henney, W.J. 2001 *RMXAA* 37 221
- White, R.J., Ghez, A.M., Reid, I.N., & Schultz, G. 1999, *ApJ*, 520, 811
- Woitas, J., Köhler, R., & Leinert, C. 2001, *A&A*, 369, 249
- Wood, K., Crosas, M., Ghez, A. 1999, *ApJ*, 516, 335
- Wood, K., Wolk, S.J., Stanek, K.Z., Leussis, G., Stassun, K., Wolff, M., & Whitney, B. 2000, *ApJ*, 542, L21